International Journal of Automotive Technology, Vol. 18, No. 4, pp. 663−670 (2017)
DOI 10.1007/s12239−017−0066−9

pISSN 1229−9138/ eISSN 1976−3832

DECOUPLED SELF-TUNING PI CONTROLLER FOR AN IDLING STOP SYSTEM APPLIED TO SCOOTERS

Pinyung Chen[1, 2], Shinhung Chang[1] and Rongshun Chen[2]*

[1]Department of Electric Propulsion, Industrial Technology Research Institute (ITRI), Hsinchu 31040, Taiwan
[2]Department of Power Mechanical Engineering, National Tsing Hua University (NTHU), Hsinchu 30013, Taiwan

(Received 25 July 2016; Revised 22 October 2016; Accepted 25 November 2016)

ABSTRACT−This paper is aimed to propose a decoupled self-tuning proportional plus integral (PI) controller with simple law for an idling stop system applied to scooters. An integrated starter generator (ISG) of the idling stop system is designed with a high efficiency permanent magnet synchronous motor (PMSM). The PMSM used as an ISG must have a high torque characteristic to ensure that the engine can be accelerated up to firing speed. A conventional and useful control algorithm named PI control is unable to handle motor current very well for dynamic load, parametric variation, and external disturbance, especially in a vehicle application. Therefore, a robust algorithm for current control in an ISG is proposed. The decoupled self-tuning PI controller based on the Lyapunov stability theorem is utilized to guarantee the control performance. Numerical simulations demonstrate the effectiveness of the proposed control algorithm. Experimental results show that the engine of a 150 cm^3 scooter can be cranked to reach firing speed by a ISG within 0.1−0.2 second. The proposed method is simple, robust, as well as stable for idling stop system, and can be effectively implemented.

KEY WORDS : Idling stop system, Scooter, Self-tuning, PI controller, Integrated starter generator

1. INTRODUCTION

The idling stop system has been used to improve the road emission on a vehicle in the past few years. The permanent magnet synchronous motor (PMSM) is a high efficiency electric machine and can provide a new selection for industrial application and vehicle engineering. The integrated starter generator (ISG) of idling stop system is designed using PMSM to connect an internal combustion engine for improving the pollution emission and to enhance fuel consumption in the scooters. For this reason, the ISG must have a good current response and suitable control gain to ensure that the engine of scooter can be accelerated up to firing speed at once when required. Especially, the idling stop system achieves the most energy-saving in frequent and complex traffic condition (Cho *et al*., 2012). In general, the ISG has twofold tasks in the idling stop system: starting up the engine and recovering the energy. This work focuses on the first task issue. In the literature, PMSMs have been used widely in driving or energy saving in industrial applications due to high torque, better power density, and high efficiency (Consoli *et al*., 2013; Kamiev *et al*., 2013). The ISG is working as a starter after a vehicle is stopping and as a generator when a vehicle is driving or idling. An idling stop system is designed to stop the engine automatically when the scooter stops, and restarts the engine simply by opening the throttle (Yanagisawa *et al*., 2010). The ISG is a high efficiency electric machine which performs both engine cranking and battery charging. In the driving control, the ISG is used to sense the rotor position to crank engine (Morandin *et al*., 2015; Rizoug *et al*., 2014). In an aircraft system, the current control techniques play an important role in power electronics. The starter-generator needs to accelerate the engine up to firing speed in the motoring mode when the system can provide the required torque in time (Degano *et al*., 2014; Arumugam *et al*., 2014; Lin *et al*., 2014; Maalouf *et al*., 2011). A direct-start direct-injection method sparks ignition engine that does not require a larger electrical starter for the conventional start-stop system (Xiao *et al*., 2015). The proportional plus integral (PI) control strategy with fuzzy system is implemented to provide a better performance for automotive sector stop-and-go in low speed urban environments (Milanes *et al*., 2012; Ting *et al*., 2015; Tseng *et al*., 2012). The control law expressed in the rotating d–q reference frame synchronize with the rotor magnet for PMSM. The current control with the feed-forward flux-weakening using a PI compensator requires an accurate value, such as the value of resistance and inductance, and a gain design is needed (Inoue *et al*., 2012; Gao *et al*., 2013). Time delays were observed in speed, voltage, and current, during acceleration and deceleration in the dynamic simulation, due to the feedback command of the PI controller. Therefore, it is difficult to deal with the

*Corresponding author. e-mail: rchen@pme.nthu.edu.tw

transient responses requirements (Kang and Kim, 2015). There are two ways to analyze the robustness; one is software in the loop simulation (SILS) for the static characteristic affection, and the other is hardware in the loop simulation (HILS) for the dynamic characteristic affection (Kwon *et al*., 2014). A Multi-level control strategy of electronic stability to achieve optimal torque distribution is estimated by an estimator. However, the estimation gain is obtained by the trial and error method, hence it is time-consuming and hard to approach robustness (Chen and Kuo, 2014). The self-organizing control method was developed to adjust the damper's slope of the sliding surface when it is subsequently incorporated into a quarter-car system under the random road. Therefore, an adjustable rule is able to achieve effective system performance by changing the parameters (Wang and Shih, 2012). The complex and nonlinear questions had been applied model-independent adaptive control theory for the self-tuning active fault-tolerant of a vehicle system. However, the online parameter require an accurate diagnosis data (Luo *et al*., 2016). The robust control design can compensate for the model uncertainty without requiring a precise model in the robustness approach. However, it requires the engineer's insights and experiences to resolve robustness performances (Kang *et al*., 2016). A self-tuning PI controller is employed to handle the high levels of uncertainties and to produce a suitable starting torque. However, it is required an adapt tuning rate to improve control performance for a permanent magnet (PM) traction machine in order to balance the unknown load torque (Gaolin *et al*., 2014; Kumbasar and Hagras, 2015; Malhotra and Gokaraju, 2014; Khorramabadi and Bakhshai, 2015). Base on the literatures mentioned, a PMSM used as an ISG with the fixed PI gain in the field-orientation control (FOC) has uncertainties, caused by parameter variations and unstructured dynamics, to crank the engine at low speed operation in the idling stop system. This work presents a decoupled self-tuning PI controller with simple law to guarantee the robustness and stability for idling stop system, and can be effectively implemented. The remainder of this paper is organized as follows. Section 2 illustrates the dynamic model description of ISG. Section 3 derives the proposed control algorithm. Simulations and experimental results are shown in Section 4 to validate the effectiveness of the proposed algorithm. Finally, conclusions are given.

2. DYNAMIC MODEL DESCRIPTION OF ISG

The PMSM used as an ISG is directly connected with engine to crank engine in an idling stop system as shown in Figure 1. For this reason, the ISG current performance has to be strict in order to achieve instant start. The electromechanical equation and dynamic model of ISG in the rotating d-q axes synchronous reference frame can be described in Equations (1) ~ (3) (Chang *et al*., 2010; Chang and Chen, 2010).

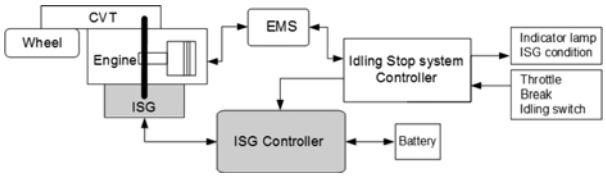

Figure 1. Overall block diagram of an idling stop system.

Table 1. Parametric definitions and values of the dynamic model.

Symbol and definitions	Values
R_{SO}: Nominal part of stator resistance	0.0126 (Ω)
L_{SO}: Nominal part of stator inductance	0.0219 (mH)
ΔR_S: Parametric variation of R_S	0.002 (Ω)
ΔL_S: Parametric variation of L_S	0.005 (mH)
i^{e*}_{ds}: Current command of d-axis	0 (A)
i^{e*}_{qs}: Current command of q-axis	30 (A)
$d1$, $d2$: The random noises	10 (bias) / 5 (magnitude)
η_p: Tuning gain of proportional term	10 (d-axis) / 0.2 (q-axis)
η_i: Tuning gain of integral term	100 (d-axis) / 20 (q-axis)
$\hat{k}_p(0)$: The initial coefficient of proportional term	0.01
$\hat{k}_i(0)$: The initial coefficient of integral term	1

where i^e_{ds} and i^e_{qs} are the d-axis and q-axis current responses of stator, respectively, v^e_{ds} and v^e_{qs} are calculated from the feedback signals of stator for the d-axis and q-axis, respectively, ϕ'_F is the permanent flux linkage, J_m is the moment of inertia of the motor, B_m is the viscous coefficient of the motor, T_L is the load torque, T_e is the motor torque response, and ω_{rm} is the mechanical rotor speed ($=\omega_e \times 2/P$), where ω_e is the electrical angular velocity, and P is the number of poles. More parametric definitions of the dynamic models for ISG under this study are listed in Table 1.

$$\frac{d}{dt}\begin{bmatrix} i^e_{ds} \\ i^e_{qs} \end{bmatrix} = \begin{bmatrix} -\frac{R_s}{L_s} & \omega_e \\ -\omega_e & -\frac{R_s}{L_s} \end{bmatrix}\begin{bmatrix} i^e_{ds} \\ i^e_{qs} \end{bmatrix} + \frac{1}{L_s}\begin{bmatrix} v^e_{ds} \\ v^e_{qs} - \omega_e \phi'_F \end{bmatrix} \quad (1)$$

$$J_m p\,\omega_{rm} + B_m\,\omega_{rm} + T_L = T_e \quad (2)$$

$$T_e = \frac{3P}{4}\phi'_F\, i^e_{qs} \quad (3)$$

In order to decouple Equation (1), the control voltage

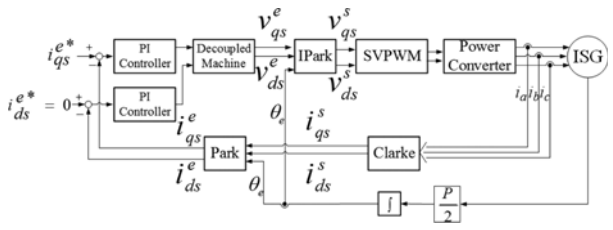

Figure 2. Block diagram of the ISG control system.

can be described,

$$v'_{ds} = v^e_{ds} + \omega_e i^e_{qs} L_s \tag{4}$$

$$v'_{qs} = v^e_{qs} - \omega_e i^e_{ds} L_s - \omega_e \phi'_F \tag{5}$$

Substituting the new control voltages Equations (4) and (5) into Equation (1), which can be rewritten as

$$\frac{d}{dt}\begin{bmatrix} i^e_{ds} \\ i^e_{qs} \end{bmatrix} = \begin{bmatrix} -\frac{R_s}{L_s} & 0 \\ 0 & -\frac{R_s}{L_s} \end{bmatrix}\begin{bmatrix} i^e_{ds} \\ i^e_{qs} \end{bmatrix} + \frac{1}{L_s}\begin{bmatrix} v^e_{ds} + \omega_e i^e_{qs} L_s \\ v^e_{qs} - \omega_e i^e_{ds} L_s - \omega_e \phi'_F \end{bmatrix} \tag{6}$$

Then, the d-q axes linear model of a ISG can be obtained as

$$\frac{d}{dt}\begin{bmatrix} i^e_{ds} \\ i^e_{qs} \end{bmatrix} = \begin{bmatrix} -\frac{R_s}{L_s} & 0 \\ 0 & -\frac{R_s}{L_s} \end{bmatrix}\begin{bmatrix} i^e_{ds} \\ i^e_{qs} \end{bmatrix} + \frac{1}{L_s}\begin{bmatrix} v'_{ds} \\ v'_{qs} \end{bmatrix} + \begin{bmatrix} d_1 \\ d_2 \end{bmatrix} \tag{7}$$

where both d_1 and d_2 are external disturbances as a random noise. The resistance and inductance of the stator are assumed to be $R_S = R_{SO} + \Delta R_S$ and $L_S = L_{SO} + \Delta L_S$.

Since the d-axis dynamics is indenpent of the q-axis dynamics in Equation (7), thus the control loop for both can be designed individually. From Equation (3), the motor torque can be obtained by the input current of the q-axis linearization i^e_{qs}, and the simple control method is similar to driving a dc motor.

Figure 2 is the block diagram of the ISG control system, where two PI controllers are applied to the current loops of d-q axes. In Figure 2, i^{e*}_{ds} and i^{e*}_{qs} the reference current command for d-axis and q-axis respectively. According to the mathematical model Equation (7), the fixed coefficients of PI controllers can be obtained based on the robust pole-placement method via state feedback to guarantee control response. Through the decoupled Equations (4) and (5), the command voltage, v^e_{qs} and v^e_{ds}, are calculated from feedback signals, ω_e, i^e_{qs}, i^e_{ds}, v'_{qs}, and v'_{ds}.

3. DECOUPLED SELF-TUNING CONTROL LAW

To obtain better current control performance, the ISG in the FOC can be simplified as a first-order system to crank engine in the idling stop system. However, the ISG model is ordinarily inaccurate due to the load disturbances, parametric variations under temperature, and the changes of operating condition. Thus, a decoupled self-tuning law is designed to provide an adjustment mechanism for the proportional and the integral coefficients under the specifications of system. The simple law of decoupled self-tuning current control in the q-axis is defined as

$$v'_{qs} = \hat{k}_p e + \hat{k}_i \int e \tag{8}$$

where $e = i^{e*}_{qs} - i^e_{qs}$. The decoupled self-tuning law can be written in Equations (9) and (10) for the proportional and the integral terms, respectively. Both η_p and η_i in the equations are positive constants and are used to determine the tuning rates.

$$\dot{\hat{k}}_p = \eta_p e^2 \operatorname{sgn}\left(\frac{\partial i^e_{qs}}{\partial v'_{qs}}\right) \tag{9}$$

$$\dot{\hat{k}}_i = \eta_i e(\int e)\operatorname{sgn}\left(\frac{\partial i^e_{qs}}{\partial v'_{qs}}\right) \tag{10}$$

In proof, the Lyapunov stability theorem is used to guarantee the effectiveness and the validity of Equations (8) ~ (10). A Lyapunov function candidate can be chosen for instance.

$$V = \frac{1}{2}e^2 \tag{11}$$

Using a direct calculation,

$$\begin{aligned} \frac{\partial V}{\partial t} &= \frac{\partial V}{\partial e}\frac{\partial e}{\partial i^e_{qs}}\frac{\partial i^e_{qs}}{\partial v'_{qs}}\frac{\partial v'_{qs}}{\partial t} \\ &= \frac{\partial V}{\partial e}\frac{\partial e}{\partial i^e_{qs}}\frac{\partial i^e_{qs}}{\partial v'_{qs}}\left(\frac{\partial v'_{qs}}{\partial k_p}\frac{\partial \hat{k}_p}{\partial t} + \frac{\partial v'_{qs}}{\partial k_i}\frac{\partial \hat{k}_i}{\partial t}\right) \\ &= -e\frac{\partial i^e_{qs}}{\partial v'_{qs}}\left(\frac{\partial v'_{qs}}{\partial k_p}\frac{\partial \hat{k}_p}{\partial t} + \frac{\partial v'_{qs}}{\partial k_i}\frac{\partial \hat{k}_i}{\partial t}\right) \\ &= -e^2\frac{\partial i^e_{qs}}{\partial v'_{qs}}\dot{\hat{k}}_p - e\frac{\partial i^e_{qs}}{\partial v'_{qs}}(\int e)\dot{\hat{k}}_i \end{aligned} \tag{12}$$

Substituting both Equations (9) and (10) into Equation (12), it is obvious that $V < 0$ while $V > 0$ can be obtained. Based on Equation (8), the adjustment coefficients $\hat{k}_p$ and $\hat{k}_i$ can deal with the tracking error close to zero. Thus, the decoupled self-tuning process would be stopped when the tracking error approaches zero. Consequently, both the coefficients $\hat{k}_p$ and $\hat{k}_i$ would converge to a fixed value to guarantee the control performance.

The decoupled self-tuning law Equations (9) and (10) are in a continuous system. To implement the control law on digital microprocessors, the decoupled self-tuning controller can be described as a discrete system,

$$\hat{k}_p(k+1) = \hat{k}_p(k) + \eta_p e^2(k)\operatorname{sgn}\left(\frac{i^e_{qs}(k) - i^e_{qs}(k-1)}{v'_{qs}(k) - v'_{qs}(k-1)}\right)\Delta t \tag{13}$$

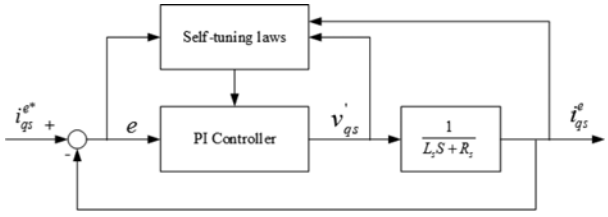

Figure 3. Architecture of the decoupled self-tuning PI controller.

$$\hat{k}_i(k+1) = \hat{k}_i(k) + \eta_i e(k)*r(k)*\mathrm{sgn}\left(\frac{i^e_{qs}(k)-i^e_{qs}(k-1)}{v'_{qs}(k)-v'_{qs}(k-1)}\right)\Delta t \tag{14}$$

where $r(k) = r(k-1) + e(k)*\Delta t$ and Δt is the sampling period. Equations (9) and (10) can be replaced by Equations (13) and (14) in a discrete system if only the sampling period can be made small enough to be implemented in a digital signal processor (DSP). Figure 3 illustrates the structure of the decoupled self-tuning PI controller in the current control of q-axis. Similarly, the d-axis decoupled self-tuning PI controller can be structured in the same way.

On the stability analysis, the system model of q-axis in Figure 3 can be considered as

$$G_p(s) = \frac{i^e_{qs}(s)}{v'_{qs}(s)} = \frac{K_a}{s\tau + 1} \tag{15}$$

where $K_a = 1 / R_S$ is the system gain and $\tau = L_S / R_S$ is the time constant. The decoupled self-tuning PI controller can be written as Equation (16) in the frequency domain.

$$G_c(s) = \hat{k}_p + \frac{\hat{k}_i}{s} \tag{16}$$

In Figure 3, given the system model Equation (15), the decoupled self-tuning PI controller Equation (16) with and $\hat{k}_p$ and $\hat{k}_i$ specified in Equations (9) and (10), the tracking error would be removed. As a result, the closed-loop system of q-axis would be stabilized since the coefficients $\hat{k}_p$ and $\hat{k}_i$ keep the system in steady state if $\hat{k}_p > -1 / K_a$ and $\hat{k}_i > 0$.

In the proof of stability using the characteristic polynomial, the transfer function of q-axis closed-loop system can be described as

$$1 + G_p(s)G_c(s) = 0 \tag{17}$$

Substituting Equations (15) and (16) into Eqution (17), the equation becomes

$$s^2 + \frac{1+\hat{k}_p K_a}{\tau}s + \frac{\hat{k}_i K_a}{\tau} = 0 \tag{18}$$

The eigenvalues of Equation (18) have to be negative to satisfy the requirement of the system stability. The stability of the system can be guaranteed by

$$\frac{1+\hat{k}_p K_a}{\tau} > 0 \quad \text{and} \quad \frac{\hat{k}_i K_a}{\tau} > 0 \tag{19}$$

or $\hat{k}_p > -1 / K_a$ and $\hat{k}_i > 0$.

4. SIMULATIONS AND EXPERIMENTAL RESULTS

In this section, simulation and experimental results are presented to verify the robustness of the proposed decoupled self-tuning PI controller for an idling stop system with uncertainties. Based on Equation (7), the simulation conditions for a given idling stop system are listed in Table 1. The idling stop system has to be robust and keep its steady state when it is subjected to an external disturbance. In this work, the external disturbances d_1 and d_2 are continuous variable current with random fluctuations in loads of d-q axes. The disturbances are much smaller than the main current, generally. The bias represents a strength of the disturbance, and the magnitude represents a variation of the disturbance. Therefore, the bias and magnitude of the disturbances depend on the previous study to be 10 and 5, respectively, as illustrated in Figure 4.

Figure 5 shows the simulation results of d-q axes current responses by different methods. The tracking errors of q-axis approaches zero within 0.15 second. The tracking

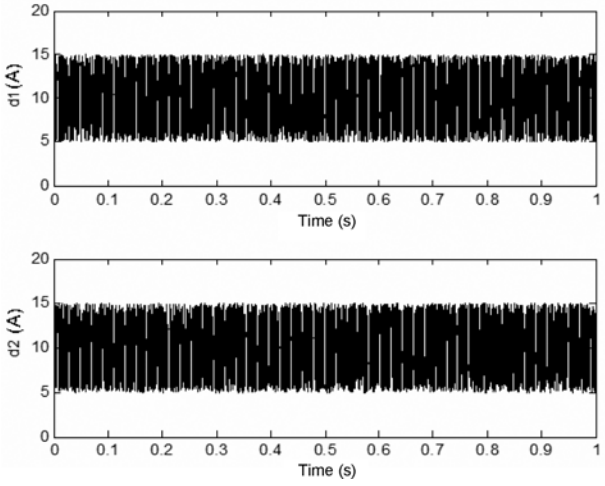

Figure 4. External disturbances, d_1 and d_2.

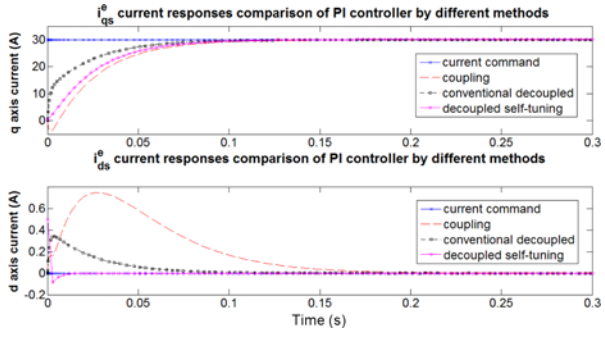

Figure 5. Simulation results of current responses by different methods.

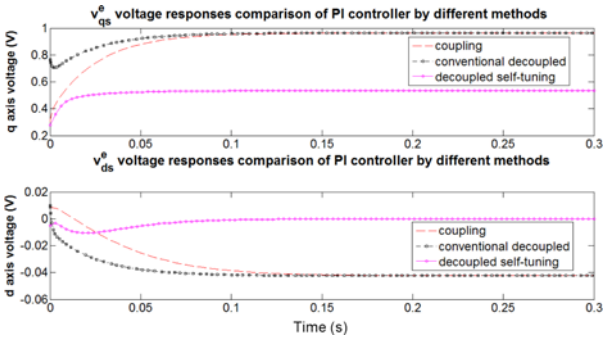

Figure 6. Simulation results of voltage responses by different methods.

errors of d-axis is the faster to approaches zero, within 0.01 second. Therefore, the proposed method has a good performance in the current responses. In the view of energy, the d-q axes voltages responses represent the input energy regulation, resulting from the feedback signals as illustrated in Figure 6. From the results of current and voltage responses, the proposed method can offer an attractive feature such as simpler implementation, faster responses, more accuracy, and energy-saving in frequent and complex traffic condition.

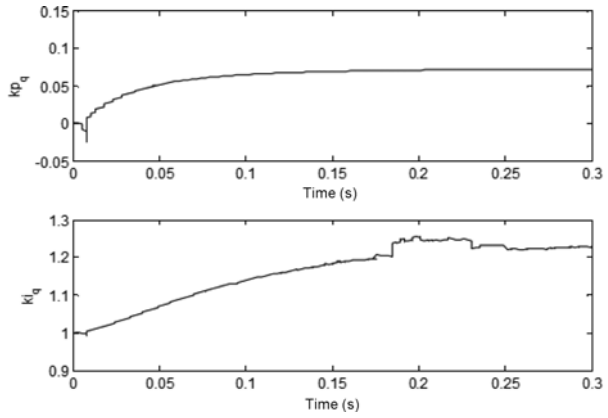

Figure 7. Variation of $\hat{k}_p$ and $\hat{k}_i$ for d-axis.

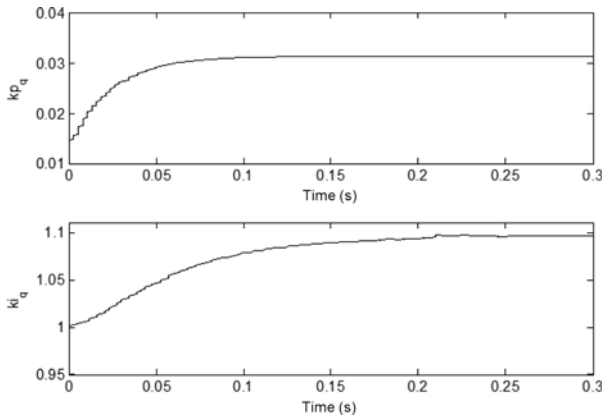

Figure 8. Variation of $\hat{k}_p$ and $\hat{k}_i$ for q-axis.

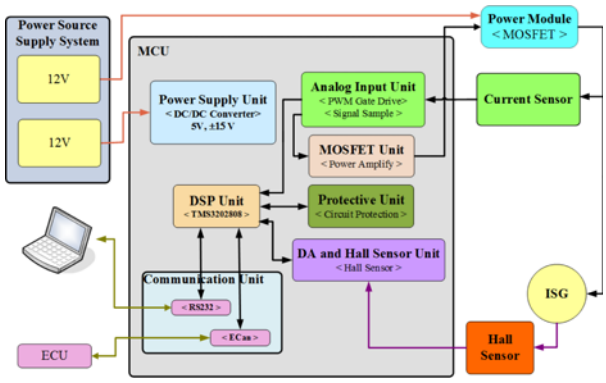

Figure 9. Experimental setup of the DSP-based controller for an ISG drive system.

The simulation results of $\hat{k}_p$ and $\hat{k}_i$ of d-q axes are shown in Figure 7 and Figure 8, respectively, where the adjusted coefficients $\hat{k}_p$ and $\hat{k}_i$ can be obtained quickly and smoothly. Obviously, the parameter $\hat{k}_p$ can be kept constant when the tracking errors approach zero.

Figure 9 illustrates the experimental setup of the DSP-based controller, in which a DSP TMS320F2808 unit and the ISG drive system are employed in the controller. All of the control methods, including a decoupled self-tuning PI controller and uncertainties term, are implemented in a DSP TMS320F2808.

In the experiments, the ISG speed is fixed at 500 rpm by an active dynamometer, based on the robust requirement. Figure 10 compares the current responses of d-axis and q-axis, respectively, using the decoupled self-tuning PI controller. From the results of simulations and experiments comparison, it is observed that the experimental results of q-axis current responses approach to the steady state faster than the results of simulation when the input command is given. On the other hand, the d-axis current responses falls nearly the desired that is the same as simulation result.

The experimental test bench for an idling stop system is shown in Figure11. Figures 12 (a) and (b) compare the experimental results of using the decoupled self-tuning and conventional PI controller, respectively, for cranking a 150

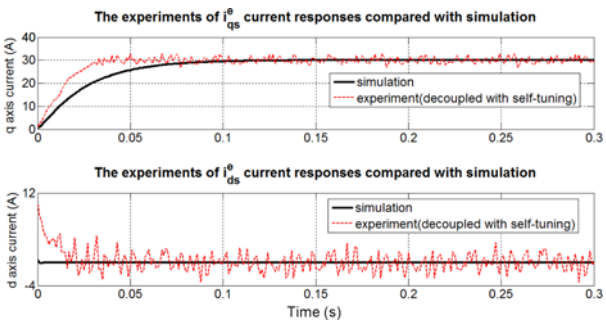

Figure 10. Experiments of current responses compared with simulations.

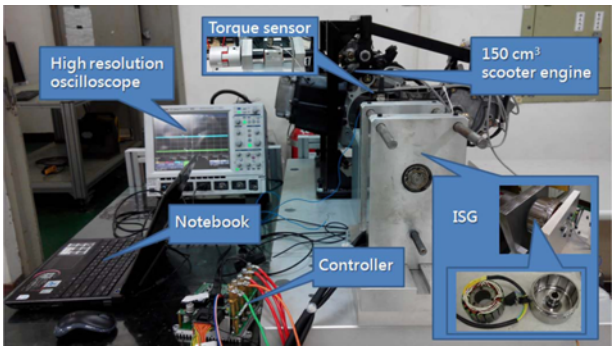

Figure 11. Experiments test bench for an idling stop system.

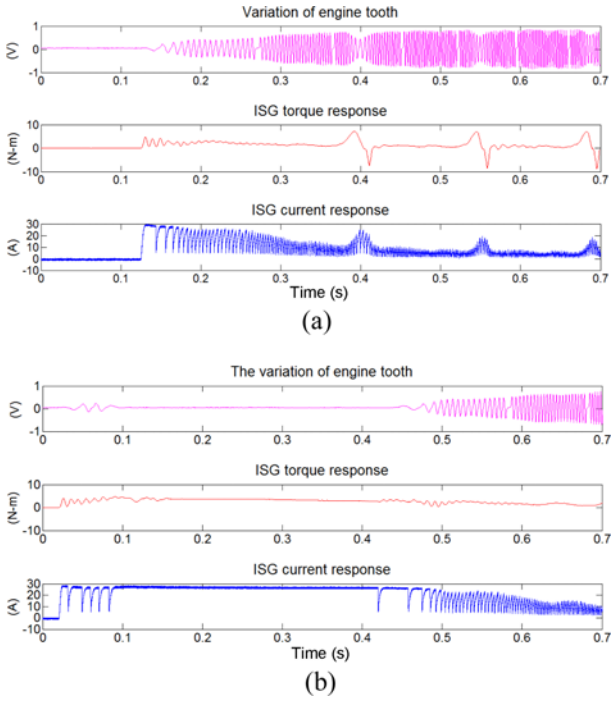

Figure 12. Comparison of experiments in a 150 cm^3 scooter by different methods: (a) Decoupled self-tuning PI controller; (b) Conventional decoupled PI controller.

cm^3 scooter by ISG. It is found that the current response of ISG to crank engine reaches the idling speed quickly when the start signal is given by the decoupled self-tuning PI controller, as shown in Figure 12 (a). On the other hand, the current response of using the conventional decoupled PI controller has some torque variations, resulting in frequent dropping down due to compression in the cylinder shown in Figure 12 (b). It is known that the conventional decoupled PI controller employs a fixed gain so that it is hardly to guarantee the robustness. As a result, the proposed method provides the best performance among the mentioned methods, and give the driver smooth and quick responses when start-up is required.

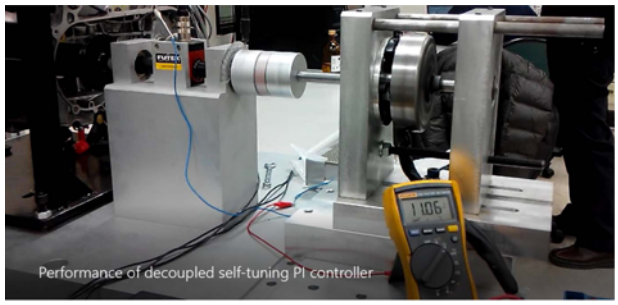

(a)

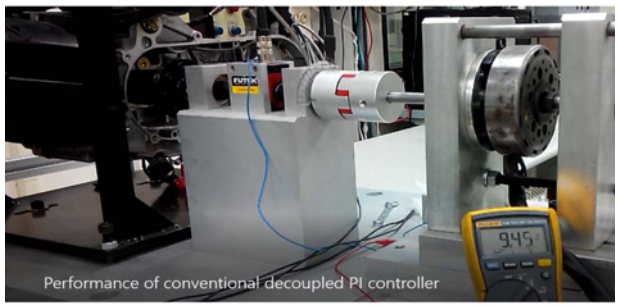

(b)

Figure 13. Comparison of power consumption experiments in a 150 cm^3 scooter by different methods: (a) Decoupled self-tuning PI controller; (b) Conventional decoupled PI controller.

Driving in urban area, the engine in a scooter or a vehicle is frequently cranked when it is equipped with a idling start system. In every time cranking, it can be deemed as a current step control. The experimental results show that the decoupled self-tuning current control can provide a quick response and a smoothing current because it can effectively suppress the starting vibration and reduce the level of required peak current. Moreover, the voltage drop when cranking the engine is significantly reduced, from 12 Vdc to 11.06 Vdc, as shown in Figure 13 (a). Thus,

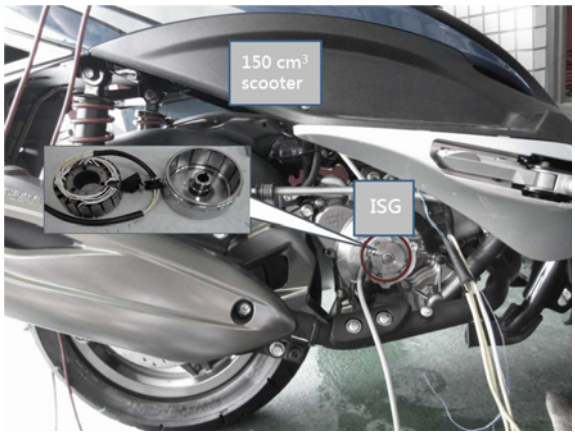

Figure 14. Configuration of ISG in an idling stop system scooter.

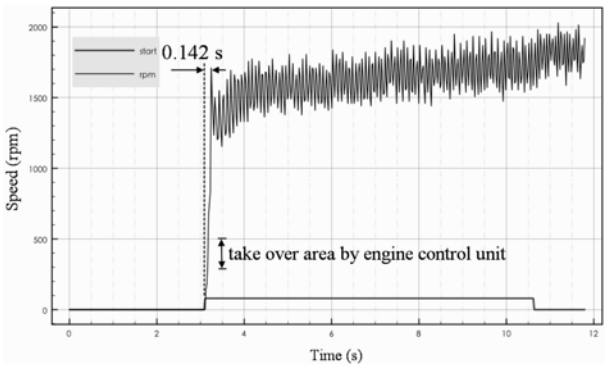

Figure 15. Experimental results of the ISG cranking performance.

the proposed method can improve discharge characteristic and enhance battery lifecycle. Conversely, the conventional decoupled PI control has a worse performance, dropping from 12 Vdc to 9.45 Vdc as illustrated Figure 13 (b).

The detail configuration of ISG in an idling stop system scooter is shown in Figure 14. Figure 15 shows the experimental result that the engine can be cranked to reach idling speed by an ISG within 0.1 - 0.2 second in a 150 cm^3 scooter, far less than the system requirements of one second.

5. CONCLUSION

This work presents a decoupled self-tuning PI controller with simple law to deal with parametric variations and external disturbances for an idling stop system applied to scooters. The current response of ISG to crank engine reaches firing speed more quickly and smoothly when the start signal is given by the proposed PI controller, comparing to a conventional method. Moreover, the self-tuning has a better advantage in energy-saving. The proposed control scheme has been implemented in a scooter idling stop system successfully. Experimental results show that the engine of a 150 cm^3 scooter can be cranked to reach its idling speed within 0.1 – 0.2 second by an ISG.

The proposed system is simple, robust, as well as stable for idling stop system. It can be effectively implemented, and extended to other idling stop control systems. Nowadays, this technology has been successfully transferred to a well-known company and is ready to mass produce.

ACKNOWLEDGEMENT–The authors would like to thank the industrial technology research institute (ITRI) of Taiwan for financial support under the project No. C301ARY330.

REFERENCES

Arumugam, P., Dusek, J., Aigbomian, A., Vakil, G., Bozhko, S., Hamiti, T., Gerada, C. and Fernando, W. (2014). Comparative design analysis of Permanent Magnet rotor topologies for an aircraft starter-generator. *IEEE 2014 Intelligent Energy and Power Systems Conf. (IEPS)*, Kyiv, Ukraine.

Chang, S. H., Chen, P. Y., Ting, Y. H. and Hung, S. W. (2010). Robust current control-based sliding mode control with simple uncertainties estimation in permanent magnet synchronous motor drive systems. *IET Electric Power Applications* **4**, **6**, 441–450.

Chang, S. H. and Chen, P. Y. (2010). Self-tuning gains of PI controllers for current control in a PMSM. *IEEE 5th Industrial Electronics and Applications Conf. (ICIEA)*, Taichung, Taiwan.

Chen, B. C. and Kuo, C. C. (2014). Electronic stability control for electric vehicle with four in-wheel motors. *Int. J. Automotive Technology* **15**, **4**, 573–580.

Cho, K., Choi, S. B., Choi, S. and Son, M. (2012). Adaptive neural network based fuzzy control for a smart idle stop and go vehicle control system. *Int. J. Automotive Technology* **13**, **5**, 791–799.

Consoli, A., Scelba, G., Scarcella, G. and Cacciato, M. (2013). An effective energy-saving scalar control for industrial IPMSM drives. *IEEE Trans. Industrial Electronics* **60**, **9**, 3658–3669.

Degano, M., Arumugam, P., Fernando, W., Yang, T., Zhang, H., Bartolo, J. B., Bozhko, S., Wheeler, P. and Gerada, C. (2014). An optimized bi-directional, wide speed range electric starter-generator for aerospace application. *IET 7th Power Electronics, Machines and Drives Conf. (PEMD)*, Manchester, UK.

Gao, F., Bozhko, S., Shen, Y. S. and Asher, G. (2013). Control design for PMM starter-generator operated in flux-weakening mode. *48th Int. Universities Power Engineering Conf. (UPEC)*, Dublin, Ireland.

Gaolin, W., Jin, X., Tielian, L., Guoqiang, Z., Hanlin, Z., Li, D. and Dianguo, X. (2014). Weight-transducerless starting torque compensation of gearless permanent-magnet traction machine for direct-drive elevators. *IEEE Trans. Industrial Electronics* **61**, **9**, 4594–4604.

Inoue, Y., Morimoto, S. and Sanada, M. (2012). Comparative study of PMSM drive systems based on current control and direct torque control in flux-weakening control region. *IEEE Trans. Industry Applications* **48**, **6**, 2382–2389.

Kamiev, K., Montonen, J., Ragavendra, M. P., Pyrhonen, J., Tapia, J. A. and Niemela, M. (2013). Design principles of permanent magnet synchronous machines for parallel hybrid or traction applications. *IEEE Trans. Industrial Electronics* **60**, **11**, 4881–4890.

Kang, D. K. and Kim, M. S. (2015). Hardware-in-the-loop simulation to evaluate the drive performance of the electric two-wheelers on a motor dynamometer. *Int. J. Automotive Technology* **16**, **6**, 1031–1040.

Kang, E., Hong, S. and Sunwoo, M. (2016). Idle speed controller based on active disturbance rejection control in diesel engines. *Int. J. Automotive Technology* **17**, **6**, 937–945.

Khorramabadi, S. S. and Bakhshai, A. (2015). Critic-based self-tuning PI structure for active and reactive power control of VSCs in microgrid systems. *IEEE Trans. Smart Grid* **6**, **1**, 92–103.

Kumbasar, T. and Hagras, H. (2015). A self-tuning zSlices-based general type-2 fuzzy PI controller. *IEEE Trans. Fuzzy Systems* **23**, **4**, 991–1013.

Kwon, J. J., Hong, T. W., Park, K., Heo, S. J., Lee, K. W., Kim, W. W., Koo, H. C. and Park, M. B. (2014). Robustness analysis of ESC ECU to characteristic variation of vehicle chassis components using HILS technique. *Int. J. Automotive Technology* **15**, **3**, 429–439.

Lin, C. K., Liu, T. H., Yu, J. T., Fu, L. C. and Hsiao, C. F. (2014). Model-free predictive current control for interior permanent-magnet synchronous motor drives based on current difference detection technique. *IEEE Trans. Industrial Electronics* **61**, **2**, 667–681.

Luo, Y., Luo, J. and Qin, Z. (2016). Model-independent self-tuning fault-tolerant control method for 4WID EV. *Int. J. Automotive Technology* **17**, **6**, 1091–1100.

Maalouf, A., Idkhajine, L., Ballois, S. L. and Monmasson, E. (2011). Field programmable gate array-based sensorless control of a brushless synchronous starter generator for aircraft application. *IET Electric Power Applications* **5**, **1**, 181–192.

Malhotra, U. and Gokaraju, R. (2014). An add-on self-tuning control system for a UPFC application. *IEEE Trans. Industrial Electronics* **61**, **5**, 2378–2388.

Milanes, V., Villagra, J., Godoy, J. and Gonzalez, C. (2012). Comparing fuzzy and intelligent PI controllers in stop-and-go manoeuvres. *IEEE Trans. Control Systems Technology* **20**, **3**, 770–778.

Morandin, M., Faggion, A. and Bolognani, S. (2015). Integrated starter-alternator with sensorless ringed-pole PM synchronous motor drive. *IEEE Trans. Industry Applications* **51**, **2**, 1485–1493.

Rizoug, N., Feld, G., Bouhali, O. and Mesbahi, T. (2014). Micro-hybrid vehicle supplied by a multi-source storage system (battery and supercapacitors): Optimal power management. *IET 7th Power Electronics, Machines and Drives Conf. (PEMD)*, Manchester, UK.

Ting, C. S., Chang, Y. N., Shi, B. W. and Lieu, J. F. (2015). Adaptive backstepping control for permanent magnet linear synchronous motor servo drive. *IET Electric Power Applications* **9**, **3**, 265–279.

Tseng, C. L., Wang, S. Y., Chien, S. C. and Chang, C. Y. (2012). Development of a self-tuning TSK-fuzzy speed control strategy for switched reluctance motor. *IEEE Trans. Power Electronics* **27**, **4**, 2141–2152.

Wang, Y. H. and Shih, M. C. (2012). Effect of a hybrid controller on ride comfort under random road excitation for a semi-active suspension system. *IMechE Part D: J. Automobile Engineering* **226**, **12**, 1640–1651.

Xiao, M., Shi, L. and Deng, K. (2015). Experimental investigation of the evaporation characteristics of the fuel in a direct-injection spark ignition engine subjected to a direct-start process. *IMechE Part D: J. Automobile Engineering* **229**, **8**, 947–957.

Yanagisawa, T., Yamanishi, T., Utsugi, K. and Nagatsuyu, T. (2010). Development of idling stop system for 125 cm^3 scooters with fuel injection. *SAE Paper No*. 2010-32-0121.